Effect of spin-orbit coupling on the effective-spin correlation in $YbMgGaO_4$

Yao-Dong Li,[1,*] Yao Shen,[1] Yuesheng Li,[2,3] Jun Zhao,[1,5] and Gang Chen[1,4,5,†]
[1]*State Key Laboratory of Surface Physics, Department of Physics, Fudan University, Shanghai 200433, China*
[2]*Department of Physics, Renmin University of China, Beijing 100872, China*
[3]*Experimental Physics VI, Center for Electronic Correlations and Magnetism, University of Augsburg, 86159 Augsburg, Germany*
[4]*Center for Field Theory and Particle Physics, Fudan University, Shanghai 200433, China*
[5]*Collaborative Innovation Center of Advanced Microstructures, Nanjing 210093, China*

(Received 25 August 2016; revised manuscript received 7 January 2018; published 5 March 2018)

Motivated by the recent experiments on the triangular lattice spin-liquid candidate $YbMgGaO_4$, we explore the effect of spin-orbit coupling on the effective-spin correlation of the Yb local moments. We point out that the anisotropic interaction between the effective spins on the nearest-neighbor bonds is sufficient to reproduce the spin-wave dispersion of the fully polarized state in the presence of strong magnetic field normal to the triangular plane. We further evaluate the effective-spin correlation at zero magnetic field within the mean-field spherical approximation. We explicitly demonstrate that the nearest-neighbor anisotropic effective-spin interaction, originating from the strong spin-orbit coupling, enhances the effective-spin correlation at the M points in the Brillouin zone. We identify these results as strong evidence for the anisotropic interaction and strong spin-orbit coupling in $YbMgGaO_4$.

DOI: 10.1103/PhysRevB.97.125105

I. INTRODUCTION

The rare-earth triangular lattice antiferromagnet $YbMgGaO_4$ was recently proposed to be a candidate for a quantum spin liquid (QSL) [1–6] and has received considerable attention [7–16]. In $YbMgGaO_4$, the Yb^{3+} ions form a perfect two-dimensional triangular lattice [1]. For the Yb^{3+} ions, the strong spin-orbit coupling (SOC) entangles the orbital angular momentum, $\mathbf{L}$ ($L = 3$), with total spin $\mathbf{s}$ ($s = 1/2$) leading to a total moment $\mathbf{J}$ ($J = 7/2$) [2,3]. Like the case in the spin-ice material $Yb_2Ti_2O_7$ [17], the crystal electric field in $YbMgGaO_4$ further splits the eight-fold degeneracy of the Yb^{3+} total moment into four Kramers' doublets. The ground-state Kramers' doublet is separated from the excited doublets by a crystal-field energy gap. At a temperature much lower than the crystal-field gap, the magnetic properties of $YbMgGaO_4$ are fully described by the ground-state Kramers' doublets [3]. The ground-state Kramers' doublet is modeled by an effective-spin-$\frac{1}{2}$ local moment $\mathbf{S}$. Therefore, $YbMgGaO_4$ is regarded as a QSL with effective-spin-$\frac{1}{2}$ local moments on a triangular lattice [2–5].

The existing experiments on $YbMgGaO_4$ have involved thermodynamic, neutron scattering, and μSR measurements [2,4–6]. The system was found to remain disordered down to 0.05 K in the recent μSR measurement [6]. The thermodynamic measurement finds a constant magnetic susceptibility in the zero-temperature limit. In the low-temperature regime, the heat capacity [1,2,5] behaves as $C_v \approx \text{constant} \times T^{0.7}$. The inelastic neutron-scattering measurements from two research groups have found the presence of broad magnetic excitation continuum [4,5]. In particular, the inelastic neutron-scattering results from Shen *et al.* clearly indicate the upper excitation edge and the *dispersive* continuum of magnetic excitations [4]. Both neutron-scattering results found a weak spectral peak at the M points in the Brillouin zone [4,5]. Based on the existing experiments, we have proposed that the spinon Fermi surface U(1) QSL gives a reasonable description of the experimental results [4].

Previously, two organic triangular antiferromagnets, κ-$(ET)_2Cu_2(CN)_3$ and $EtMe_3Sb[Pd(dmit)_2]_2$, were proposed to be QSLs [18–21]. These two materials are in the weak Mott regime, where the charge fluctuation is strong. It was then suggested that the four-spin ring exchange interaction due to the strong charge fluctuation may destabilize the magnetic order and favor a QSL ground state [22,23]. Unlike the organic counterparts, $YbMgGaO_4$ is in the strong Mott regime [2,3]. The $4f$ electrons of the Yb^{3+} ion is very localized spatially. As a result, the physical mechanism for the QSL ground state in this new material is deemed to be quite different. The new ingredients of the new material are believed to be the strong SOC and the spin-orbit-entangled nature of the Yb^{3+} local moment. It was pointed out that the spin-orbit entanglement leads to highly anisotropic interactions between the Yb local moments [3,24–26]. The anisotropic effective-spin interaction is shown to enhance the quantum fluctuation and suppress the magnetic order in a large parameter regime where the QSL may be located [3]. On the fundamental side, it was recently argued that, as long as the time-reversal symmetry is preserved, the ground state of a spin-orbit-coupled Mott insulator with an odd number of electrons per cell must be exotic [27]. This theoretical argument implies that the spin-orbit-coupled Mott insulator can in principle be a candidate for spin liquids. $YbMgGaO_4$ falls into this class and is actually the first such material.

*Present address: Department of Physics, University of California, Santa Barbara, California 93106, USA.
†gangchen.physics@gmail.com; gchen_physics@fudan.edu.cn

 ©2018 American Physical Society

More recently, Ref. [5] introduced the XXZ exchange interactions on both nearest-neighbor and next-nearest-neighbor sites to account for the spin-wave dispersion in the strong magnetic field and the weak peak at the M points in the effective-spin correlations. The authors further suggested the further neighbor competing exchange interactions as the possible mechanism for the QSL in $YbMgGaO_4$. In this paper, however, we focus on the anisotropic effective-spin interactions on the nearest-neighbor sites. After justifying the underlying microscopics that support the nearest-neighbor anisotropic model, we demonstrate that the nearest-neighbor model is sufficient to reproduce the spin-wave dispersion of the polarized state in a strong magnetic field. With the nearest-neighbor anisotropic model, we further show that the effective-spin correlation also develops a peak at the M points. Therefore, we think the nearest-neighbor anisotropic model captures the essential physics for $YbMgGaO_4$.

The remaining part of the paper is outlined as follows: In Sec. II, we describe some of the details about the microscopics of the interactions between the Yb local moments. In Sec. III, we compare the spin-wave dispersion of the nearest-neighbor anisotropic interactions in a strong field with the existing experimental data. In Sec. IV, we evaluate the effective-spin correlation from the effective-spin models with and without the anisotropic interaction. Finally in Sec. V, we conclude with a discussion.

II. ANISOTROPIC INTERACTION FOR EFFECTIVE SPINS

Compared to the organic spin-liquid candidates [18–21], $YbMgGaO_4$ is in the strong Mott regime, and the charge fluctuation is rather weak. Therefore, the four-spin ring exchange, which is a higher-order perturbative process than the nearest-neighbor pairwise interaction, is strongly suppressed. In previous work [2,3], we proposed the following generic pairwise effective-spin interaction for the nearest-neighbor Yb moments in $YbMgGaO_4$:

$$\begin{aligned}\mathcal{H} = &\sum_{\langle \mathbf{r}\mathbf{r}'\rangle} J_{zz} S^z_{\mathbf{r}} S^z_{\mathbf{r}'} + J_{\pm}(S^+_{\mathbf{r}} S^-_{\mathbf{r}'} + S^-_{\mathbf{r}} S^+_{\mathbf{r}'}) \\ &+ J_{\pm\pm}(\gamma_{\mathbf{r}\mathbf{r}'} S^+_{\mathbf{r}} S^+_{\mathbf{r}'} + \gamma^*_{\mathbf{r}\mathbf{r}'} S^-_{\mathbf{r}} S^-_{\mathbf{r}'}) \\ &- \frac{i J_{z\pm}}{2}[(\gamma^*_{\mathbf{r}\mathbf{r}'} S^+_{\mathbf{r}} - \gamma_{\mathbf{r}\mathbf{r}'} S^-_{\mathbf{r}}) S^z_{\mathbf{r}'} \\ &+ S^z_{\mathbf{r}}(\gamma^*_{\mathbf{r}\mathbf{r}'} S^+_{\mathbf{r}'} - \gamma_{\mathbf{r}\mathbf{r}'} S^-_{\mathbf{r}'})], \qquad (1)\end{aligned}$$

where $S^{\pm}_{\mathbf{r}} = S^x_{\mathbf{r}} \pm i S^y_{\mathbf{r}}$, and $\gamma_{\mathbf{r}\mathbf{r}'} = \gamma_{\mathbf{r}'\mathbf{r}} = 1, e^{i2\pi/3}, e^{-i2\pi/3}$ are the phase factors for the bond $\mathbf{r}\mathbf{r}'$ along the $\mathbf{a_1}, \mathbf{a_2}, \mathbf{a_3}$ directions (see Fig. 1). The $J_{\pm\pm}$ and $J_{z\pm}$ terms of Eq. (1) are anisotropic interactions arising naturally from the strong SOC. Due to the SOC, the effective spins inherit the symmetry operation of the space group, so there are bond-dependent $J_{\pm\pm}$ and $J_{z\pm}$ interactions.

Our generic model in Eq. (1) contains the contribution from all microscopic processes that include the direct $4f$-electron exchange, the indirect exchange through the intermediate oxygen ions, and the dipole-dipole interaction. Any further-neighbor interaction is neglected in our generic model. Like the ring exchange, the further neighbor superexchange may involve higher-order perturbative processes via multiple steps of electron tunnelings than the nearest-neighbor interactions. Even though the further neighbor superexchange interaction can be mediated by the direct electron hoppings between these sites, the contribution should be very small due to the very localized nature of the $4f$ electron wave function. The remaining contribution is the further neighbor dipole-dipole interaction. For the next-nearest neighbors, the dipole-dipole interaction is estimated to be ~0.01–0.02 K and is thus one or two orders of magnitude smaller than the nearest-neighbor interactions. Therefore, we neglect further neighbor interactions and only keep the nearest-neighbor interactions in Eq. (1).

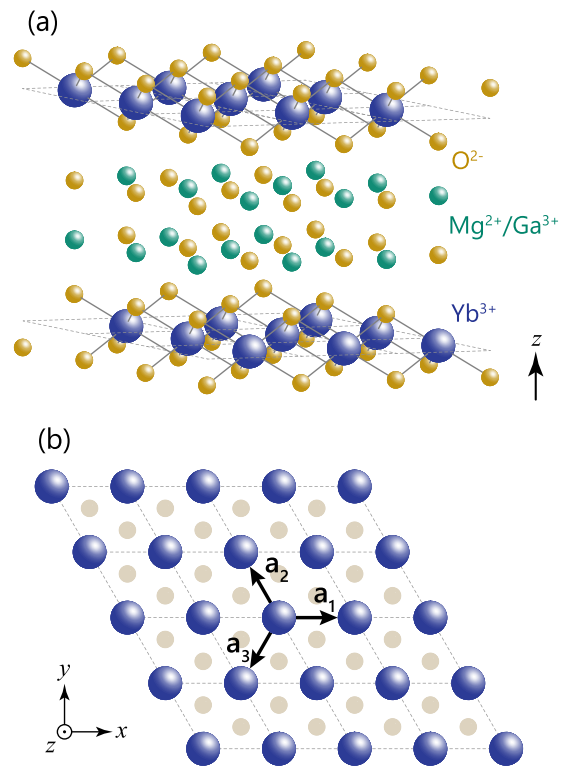

FIG. 1. (a) Crystal structure of $YbMgGaO_4$. Mg and Ga ions form the nonmagnetic layer. (b) Yb triangular layer.

The large chemical difference prohibits the Ga or Mg contamination in the Yb layers. The Yb layers are kept clean, and there is little disorder in the exchange interaction. Although there exists Ga-Mg mixing in the nonmagnetic layers, the exchange path that they involve would be Yb-O-Ga-O-Yb or Yb-O-Mg-O-Yb (see Fig. 1). This exchange path is a higher-order perturbative process than the Yb-O-Yb one and thus can be neglected. If this mechanism is primary, we do not expect the Ga-Mg mixing in the nonmagnetic layers to cause much exchange disorder within the Yb layers. If the crystal electric field of the Yb ion is strongly influenced by the Ga-Mg mixing in the nonmagnetic layers [13], then the exchange may be more affected. The recent polarized-neutron-scattering experiment [15], however, suggests that despite the presence of Ga-Mg mixing, the exchange disorder is not quite significant. Moreover, the Ga-Mg disorder in $YbMgGaO_4$ is fundamentally different from the Cu-Zn disorder in herbertsmithite [28–31]. In the latter case, the Cu disorder carries a magnetic moment and directly couples to the spin in the Cu layers.

The XXZ limit of our generic model has already been studied in some of the early works [32,33]. It was shown that the magnetic-ordered ground state was obtained for all parameter regions in the XXZ limit. To obtain a disordered ground state for the generic model, it is necessary to have the $J_{\pm\pm}$ and $J_{z\pm}$ interactions. In Ref. [3], we have shown that the 120° magnetic order in the XXZ limit is actually destabilized by the enhanced quantum fluctuation when the anisotropic $J_{\pm\pm}$ and $J_{z\pm}$ interactions are introduced.

III. SPIN-WAVE DISPERSION IN STRONG MAGNETIC FIELD

The nearest-neighbor interaction between the Yb local moments are of the order of several kelvin [2]; as a result, a moderate magnetic field in the laboratory is sufficient for polarizing the local moment [3]. Under the linear spin-wave approximation, the spin-wave dispersion in the presence of the strong external magnetic field is given as [3]

$$\omega_z(\mathbf{k}) = \left\{\left[g_z\mu_B B_z - 3J_{zz} + 2J_\pm \sum_{i=1}^{3}\cos(\mathbf{k}\cdot\mathbf{a}_i)\right]^2 - 4J_{\pm\pm}^2\left|\cos(\mathbf{k}\cdot\mathbf{a}_1) + e^{-i\frac{2\pi}{3}}\cos(\mathbf{k}\cdot\mathbf{a}_2) + e^{i\frac{2\pi}{3}}\cos(\mathbf{k}\cdot\mathbf{a}_3)\right|^2\right\}^{1/2}, \tag{2}$$

where g_z and B_z are the Landé factor and the magnetic field along the z direction, respectively. Note that the dispersion in Eq. (2) is *independent* of $J_{z\pm}$ for the magnetic field along the z direction; this is an *artifact* of the *linear* spin-wave approximation.

In the recent experiment in Ref. [5], a magnetic field of 7.8 T normal to the Yb plane at 0.06 K, a gapped magnon band structure is observed. In Fig. 2, we compare our theoretical result with a *tentative* choice of exchange couplings in Eq. (2) with the experimental results from Ref. [5]. Since the error bar is not known from Ref. [5], judging from the extension of the bright region in Fig. 2(a), we would think that the agreement between the theoretical result and the experimental result is reasonable. Here, we have to mention that the dispersion plotted in Fig. 2 is not quite sensitive to the choice of $J_{\pm\pm}$. Therefore, we expect it is better to combine the spin-wave dispersion for several field orientations and to extract the exchange couplings more accurately. For an arbitrary external field in the xz plane, the Hamiltonian is given by

$$\mathcal{H}_{xz} = \mathcal{H} - \sum_{\mathbf{r}} \mu_B\left[g_x B_x S_{\mathbf{r}}^x + g_z B_z S_{\mathbf{r}}^z\right]. \tag{3}$$

Since $g_x \neq g_z$, the uniform magnetization, $\mathbf{m} \equiv \langle \mathbf{S}_{\mathbf{r}}\rangle$, is generally not parallel to the external magnetic field. For $B_x \equiv B\sin\theta$ and $B_z \equiv B\cos\theta$, the magnetization is given by

$$\mathbf{m} = m(\hat{x}\sin\theta' + \hat{z}\cos\theta'), \tag{4}$$

where $\tan\theta' = (g_x/g_z)\tan\theta$. At a sufficiently large magnetic field, all the moments are polarized along the direction defined by θ'. In the linear spin-wave theory for this polarized state, we choose the magnetization to be the quantization axis for the Holstein–Primakoff transformation,

$$\mathbf{S}_{\mathbf{r}}\cdot\frac{\mathbf{m}}{|\mathbf{m}|} \equiv \frac{1}{2} - a_{\mathbf{r}}^\dagger a_{\mathbf{r}}, \tag{5}$$

$$\mathbf{S}_{\mathbf{r}}\cdot\hat{y} \equiv \frac{1}{2}(a_{\mathbf{r}} + a_{\mathbf{r}}^\dagger), \tag{6}$$

$$\mathbf{S}_{\mathbf{r}}\cdot\left(\frac{\mathbf{m}}{|\mathbf{m}|}\times\hat{y}\right) \equiv \frac{1}{2i}(a_{\mathbf{r}} - a_{\mathbf{r}}^\dagger), \tag{7}$$

where $a_{\mathbf{r}}^\dagger$ ($a_{\mathbf{r}}$) is the creation (annihilation) operator for the Holstein–Primakoff boson. In the linear spin-wave approximation, we plug the Holstein–Primakoff transformation into $\mathcal{H}_{xz}$ and keep the quadratic part of the Holstein–Primakoff bosons. The spin-wave dispersion is obtained by solving the linear spin-wave Hamiltonian and is given by

$$\begin{aligned}\omega_{xz}(\mathbf{k}) = \Bigg\{\Bigg\{&g_x\mu_B B_x\sin\theta' + g_z\mu_B B_z\cos\theta' - 6J_\pm\sin^2\theta' - 3J_{zz}\cos^2\theta' + \cos(\mathbf{k}\cdot\mathbf{a}_1)\\ &\times\left[\frac{J_\pm}{2}(3+\cos 2\theta') - J_{\pm\pm}\sin^2\theta' + \frac{J_{zz}}{2}\sin^2\theta'\right]\\ &+\cos(\mathbf{k}\cdot\mathbf{a}_2)\left[\frac{J_\pm}{2}(3+\cos 2\theta') + \frac{J_{\pm\pm}}{2}\sin^2\theta' + \frac{J_{zz}}{2}\sin^2\theta' + \frac{\sqrt{3}}{4}J_{z\pm}\sin 2\theta'\right]\\ &+\cos(\mathbf{k}\cdot\mathbf{a}_3)\left[\frac{J_\pm}{2}(3+\cos 2\theta') + \frac{J_{\pm\pm}}{2}\sin^2\theta' + \frac{J_{zz}}{2}\sin^2\theta' - \frac{\sqrt{3}}{4}J_{z\pm}\sin 2\theta'\right]\Bigg\}^2\\ &-\Bigg|\cos(\mathbf{k}\cdot\mathbf{a}_1)\left[J_\pm\sin^2\theta' - J_{\pm\pm}(1+\cos^2\theta') - iJ_{z\pm}\sin\theta' - \frac{J_{zz}}{2}\sin^2\theta'\right]\\ &+\cos(\mathbf{k}\cdot\mathbf{a}_2)\Bigg[J_\pm\sin^2\theta' + \frac{J_{\pm\pm}}{4}(3+\cos 2\theta' - 4i\sqrt{3}\cos\theta')\\ &-\frac{J_{zz}}{2}\sin^2\theta' + \frac{J_{z\pm}}{4}(2i\sin\theta' - \sqrt{3}\sin 2\theta')\Bigg]\end{aligned}$$

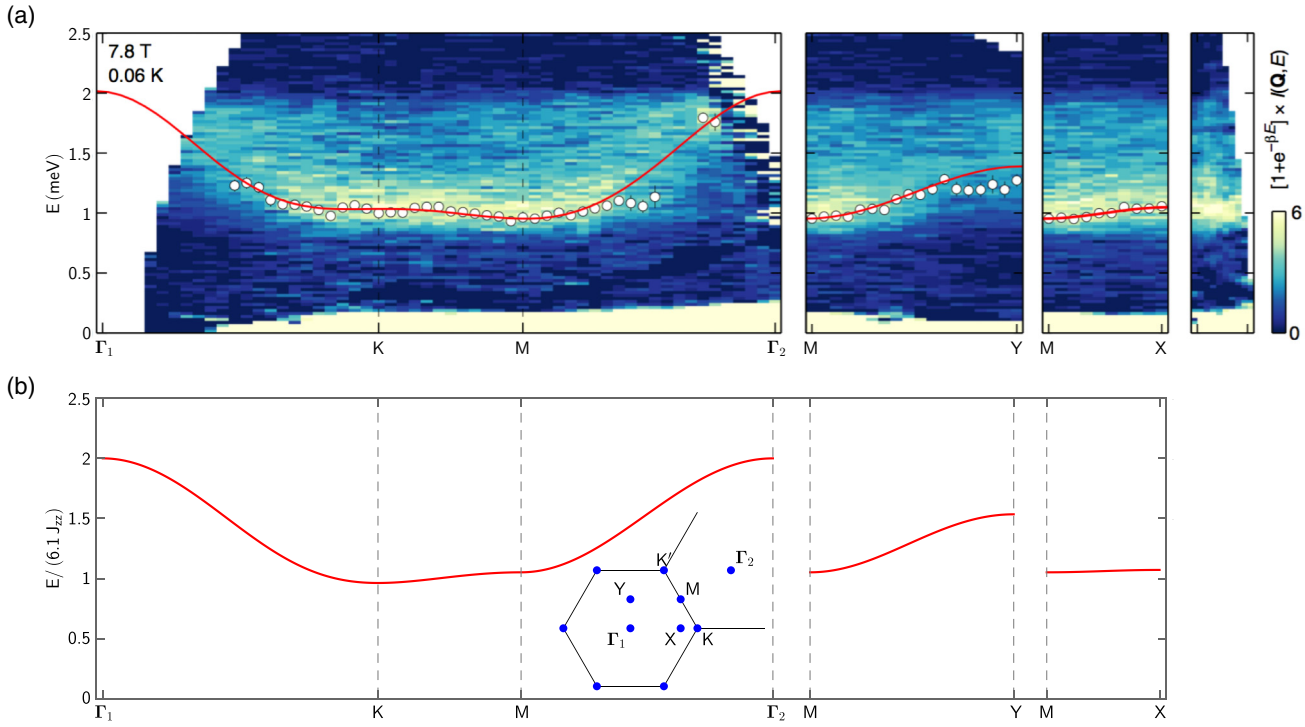

FIG. 2. (a) Experimental spin-wave dispersion in the presence of an external field along the z direction with a field strength of 7.8 T at 0.06 K (adapted from the arXiv version of Ref. [5]). According to Ref. [5], the white circles indicate the location of maximum intensity. The error bar, however, is not indicated in the plot. The red lines show a fit to the spin-wave dispersion relation that is obtained after including both nearest-neighbor and next-nearest-neighbor XXZ exchange interactions [5]. (b) Theoretical spin-wave dispersion according to nearest-neighbor anisotropic exchange model (1), where we set $J_{\pm}/J_{zz} = 0.66$, $J_{\pm\pm}/J_{zz} = 0.34$, and $h/J_{zz} = 10.5$. The analytical expression of the dispersion is given in Eq. (2). The inset of panel (b) is the Brillouin zone.

$$+ \cos(\mathbf{k}\cdot\mathbf{a}_3)\Big[J_{\pm}\sin^2\theta' + \frac{J_{\pm\pm}}{4}(3+\cos 2\theta' + 4i\sqrt{3}\cos\theta') - \frac{J_{zz}}{2}\sin^2\theta' + \frac{J_{z\pm}}{4}(2i\sin\theta' + \sqrt{3}\sin 2\theta')\Big]\Big|^2\Big\}^{1/2}. \tag{8}$$

Likewise, for the field within the xy plane, the Hamiltonian is given by

$$\mathcal{H}_{xy} = \mathcal{H} - \sum_{\mathbf{r}} \mu_B\big[g_x B_x S^x_{\mathbf{r}} + g_y B_y S^y_{\mathbf{r}}\big]. \tag{9}$$

Now because of the threefold on-site symmetry, $g_x = g_y$. The magnetization is parallel to the external magnetic field. For $B_x \equiv B\cos\phi$ and $B_y \equiv B\sin\phi$, the magnetization is $\mathbf{m} = m(\hat{x}\cos\phi + \hat{y}\sin\phi)$, and the corresponding spin-wave dispersion in the strong-field limit is given by

$$\begin{aligned}\omega_{xy}(\mathbf{k}) = \Big\{\Big\{&g_x\mu_B B_x\cos\phi + g_y\mu_B B_y\sin\phi - 6J_{\pm} + \cos(\mathbf{k}\cdot\mathbf{a}_1)\Big(J_{\pm} + \frac{J_{zz}}{2} - J_{\pm\pm}\cos 2\phi\Big)\\ &+ \cos(\mathbf{k}\cdot\mathbf{a}_2)\Big[J_{\pm} + \frac{J_{zz}}{2} + J_{\pm\pm}\cos\Big(2\phi - \frac{\pi}{3}\Big)\Big]\\ &+ \cos(\mathbf{k}\cdot\mathbf{a}_3)\Big[J_{\pm} + \frac{J_{zz}}{2} + J_{\pm\pm}\cos\Big(2\phi + \frac{\pi}{3}\Big)\Big]\Big\}^2 - \Big|\cos(\mathbf{k}\cdot\mathbf{a}_1)\Big(J_{\pm} - \frac{J_{zz}}{2} - J_{\pm\pm}\cos 2\phi + iJ_{z\pm}\cos\phi\Big)\\ &+ \cos(\mathbf{k}\cdot\mathbf{a}_2)\Big[J_{\pm} - \frac{J_{zz}}{2} + J_{\pm\pm}\cos\Big(2\phi + \frac{\pi}{3}\Big) - iJ_{z\pm}\cos\Big(\phi - \frac{\pi}{3}\Big)\Big]\\ &+ \cos(\mathbf{k}\cdot\mathbf{a}_3)\Big[J_{\pm} - \frac{J_{zz}}{2} + J_{\pm\pm}\cos\Big(2\phi - \frac{\pi}{3}\Big) - iJ_{z\pm}\cos\Big(\phi + \frac{\pi}{3}\Big)\Big]\Big|^2\Big\}^{1/2}.\end{aligned} \tag{10}$$

IV. EFFECTIVE-SPIN CORRELATION

In both Refs. [4] and [5], a weak spectral peak at the M points is found in the inelastic-neutron-scattering data. This result indicates that the interaction between the Yb local moments enhances the correlation of the effective spins at the M points. Actually, in Ref. [3], we have already shown that, the anisotropic $J_{\pm\pm}$ and $J_{z\pm}$ interactions, if they are significant, would favor a stripe magnetic order with an ordering wave vector at the M points [34]. This theoretical result immediately means that the anisotropic $J_{\pm\pm}$ and $J_{z\pm}$ interactions would enhance the effective-spin correlation at the M points. In the following, we demonstrate explicitly that the generic model in Eq. (1) with the anisotropic nearest-neighbor interactions does enhance the effective-spin correlation at the M points. We start from the mean-field partition function of the system,

$$\begin{aligned}\mathcal{Z} &= \int \mathcal{D}[\mathbf{S_r}] \prod_{\mathbf{r}} \delta\left(\mathbf{S}_{\mathbf{r}}^2 - S^2\right) e^{-\beta\mathcal{H}} \\ &= \int \mathcal{D}[\mathbf{S_r}]\mathcal{D}[\lambda_{\mathbf{r}}]\, e^{-\beta\mathcal{H}+\sum_{\mathbf{r}}\lambda_{\mathbf{r}}[\mathbf{S}_{\mathbf{r}}^2 - S^2]} \\ &\equiv \int \mathcal{D}[\mathbf{S_r}]\mathcal{D}[\lambda_{\mathbf{r}}]\, e^{-\mathcal{S}_{\text{eff}}[\beta,\lambda_{\mathbf{r}}]}, \end{aligned} \tag{11}$$

where $\mathcal{H}$ is given in Eq. (1), $\mathcal{S}_{\text{eff}}$ is the effective action that describes the effective-spin interaction, and $\lambda_{\mathbf{r}}$ is the local Lagrange multiplier that imposes the local constraint with $|\mathbf{S_r}|^2 = S^2$. Although this mean-field approximation does not give the quantum ground state, it does provide a qualitative understanding of the relationship between the effective-spin correlation and the microscopic spin interactions.

To evaluate the effective-spin correlation, we adopt here a spherical approximation [35] by replacing the local constraint with a global one such that $\sum_{\mathbf{r}} |\mathbf{S_r}|^2 = N_{\text{site}} S^2$, where N_{site} is the total number of lattice sites. This approximation is equivalent to choosing a uniform Lagrange multiplier with $\lambda_{\mathbf{r}} \equiv \lambda$. It has been shown that the spin correlations determined from classical Monte Carlo simulation are described quantitatively within this scheme [35]. The validity of this method is justified by the fact that the thermal fluctuation at finite temperatures softens the local spin constraint. This method was quoted as the self-consistent Gaussian approximation in Ref. [15].

In the momentum space, we define

$$S_{\mathbf{r}}^{\mu} \equiv \frac{1}{\sqrt{N_{\text{site}}}} \sum_{\mathbf{k}\in\text{BZ}} S_{\mathbf{k}}^{\mu}\, e^{i\mathbf{k}\cdot\mathbf{r}}, \tag{12}$$

and the effective action is given by

$$\begin{aligned}\mathcal{S}_{\text{eff}}[\beta,\lambda] = &\sum_{\mathbf{k}\in\text{BZ}} \beta[\mathcal{J}_{\mu\nu}(\mathbf{k}) + \Delta(\beta)\delta_{\mu\nu}] \\ &\times S_{\mathbf{k}}^{\mu}\, S_{-\mathbf{k}}^{\nu} - \beta N_{\text{site}}\Delta(\beta) S^2, \end{aligned} \tag{13}$$

where we have placed $\lambda \equiv -\beta\Delta(\beta)$ in a saddle-point approximation, $\mu, \nu = x, y, z$, and $\mathcal{J}_{\mu\nu}(\mathbf{k})$ is a 3×3 exchange matrix that is obtained by Fourier transforming the exchange couplings. Note the XXZ part of the spin interactions only appears in the diagonal part of $\mathcal{J}_{\mu\nu}(\mathbf{k})$ while the anisotropic $J_{\pm\pm}$ and $J_{z\pm}$ interactions are also present in the off-diagonal part. Thus, the effective-spin correlation is given as

$$\langle S_{\mathbf{k}}^{\mu}\, S_{-\mathbf{k}}^{\nu}\rangle = \frac{1}{\beta}[\mathcal{J}(\mathbf{k}) + \Delta(\beta)\mathbb{1}_{3\times 3}]_{\mu\nu}^{-1}, \tag{14}$$

where $\mathbb{1}_{3\times 3}$ is a 3×3 identity matrix.

The saddle-point equation is obtained by integrating out the effective spins in the partition function and is given by

$$\sum_{\mathbf{k}\in\text{BZ}} \sum_{\mu} \frac{1}{\beta}[\mathcal{J}(\mathbf{k}) + \Delta(\beta)\mathbb{1}_{3\times 3}]_{\mu\mu}^{-1} = N_{\text{site}} S^2, \tag{15}$$

from which we determine $\Delta(\beta)$ and the effective-spin correlation in Eq. (14).

The results of the effective-spin correlations are presented in Fig. 3. In the absence of the $J_{\pm\pm}$ and $J_{z\pm}$ interactions, the correlation function is peaked at the K points. This result is understood since the XXZ model that favors the 120° state would simply enhance the effective-spin correlation at the K points that correspond to the ordering wave vectors of the 120° state. After we include the $J_{\pm\pm}$ and $J_{z\pm}$ interactions, the peak of the correlation function is switched to the M points [see Fig. 3(d)]. In the appendix, we provide the spin correlations for more parameter choices of the anisotropic exchange couplings $J_{\pm\pm}$ and $J_{z\pm}$. This suggests that it is sufficient to have the $J_{\pm\pm}$ and $J_{z\pm}$ interactions in the nearest-neighbor model to account for the peak at the M points in the neutron-scattering results.

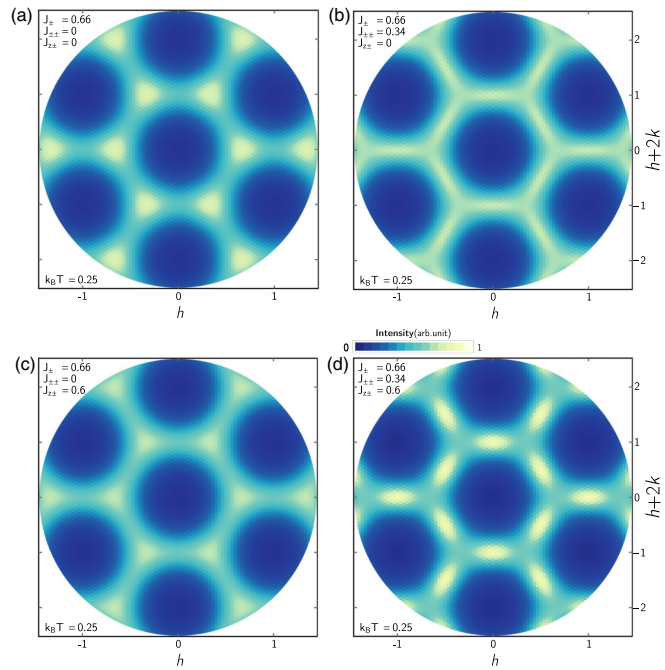

FIG. 3. Contour plot of effective-spin correlation $\langle S_{\mathbf{k}}^{+}\, S_{-\mathbf{k}}^{-}\rangle$ in momentum space. The correlation function is computed from the nearest-neighbor model (1), with parameters in units of J_{zz} indicated. Without the anisotropic exchanges, the spectral weight peaks around K. The anisotropic $J_{\pm\pm}$ and $J_{z\pm}$ interactions can switch the peak to M.

V. DISCUSSION

Instead of invoking further-neighbor interactions in Ref. [5], we focus on the anisotropic spin interaction on the nearest-

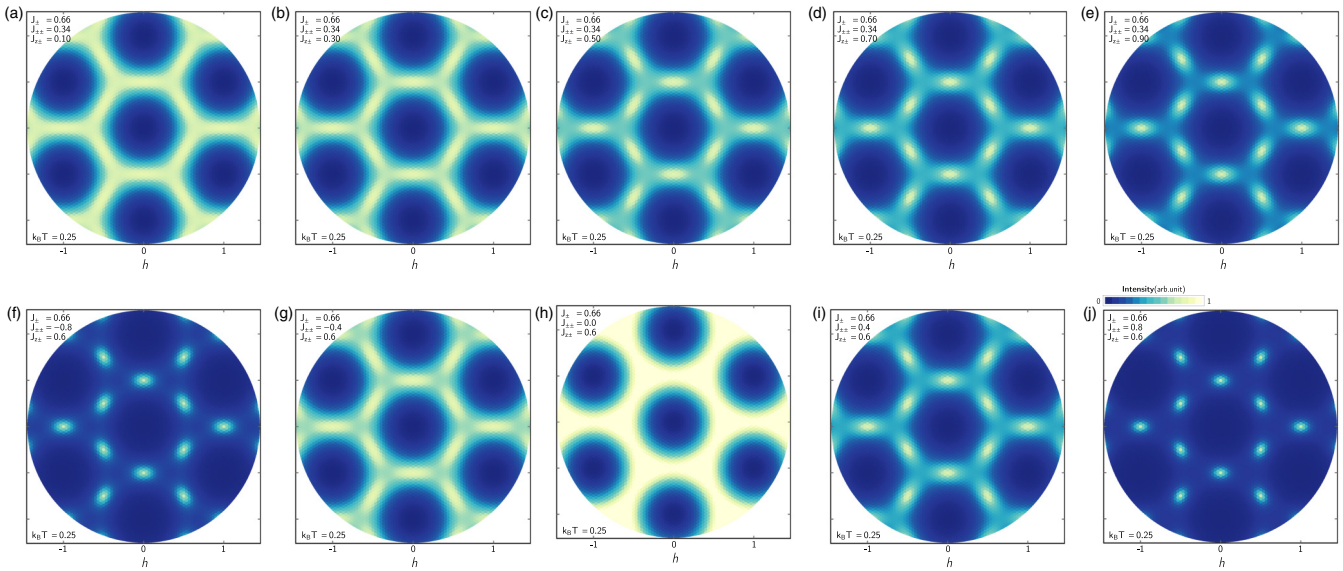

FIG. 4. Contour plot of effective-spin correlation $\langle S^+_{\mathbf{k}}\, S^-_{-\mathbf{k}}\rangle$ in momentum space. In the plot, we set J_{zz} as the energy unit, i.e., $J_{zz} = 1$. We choose parameters on the horizontal and vertical lines through the optimal point $(J_{\pm\pm}, J_{z\pm}) = (0.34J_{zz}, 0.6J_{zz})$ in the $J_{\pm} = 0.66J_{zz}$ plane of phase diagram.

neighbor bonds to account for the spin-wave dispersion of the polarized state in the strong magnetic field and the effective-spin correlation in $YbMgGaO_4$. The bond-dependent interaction is a natural and primary consequence of the strong SOC in the system. As for further-neighbor interactions, although they generally exist, they should be rather weak for Yb^{3+} ions. That the next-nearest-neighbor interactions in Refs. [5,36] are quite large is surprising. Thus, it is reasonable to keep only nearest-neighbor interactions.

We have recently proposed that the spinon Fermi surface U(1) QSL provides a consistent explanation for the experimental results in $YbMgGaO_4$ [4,8]. We pointed out that the particle-hole excitation of a simple noninteracting spinon Fermi sea already gives both the broad continuum and the upper excitation edge in the inelastic-neutron-scattering spectrum. In Ref. [9], we variationally optimized the energy against the trial ground-state wave function that is constructed from a more generic spinon Fermi surface mean-field state and directly computed the correlation function of the local moments with respect to the variational ground state. Finally, we note that there is a recent proposal that has a different emphasis on the second-neighbor exchange coupling [36].

ACKNOWLEDGMENTS

G.C. acknowledges Dr. Martin Mourigal for discussions about the energy resolution. G.C. thanks Dr. Zhong Wang at IAS of Tsinghua University and Dr. Nanlin Wang at ICQM of Peking University for their hospitality during my visit in August 2016. This work was supported by the Ministry of Science and Technology of China through Grant No. 2016YFA0301001 (G.C.), the Start-up Funds and the Program of First-Class Construction of Fudan University (G.C.), and the Thousand-Youth-Talent Program (G.C.) of China.

APPENDIX A: SPIN CORRELATIONS WITH MORE PARAMETER CHOICES

Here we provide results of the spin correlation derived from the generic model given in the main text for a larger set of parameters. Such information should facilitate a systematic comparison between theory and experiment. Again, due to the limited experimental information (e.g., we do not directly obtain $J_{z\pm}$ from the neutron-scattering results), the results here merely emphasize the importance of the anisotropic spin interactions.

The results are shown in Fig. 4. The evolution of the spin correlations with the varying parameters confirms the classical phase diagram of the model. For large $J_{z\pm}$ or $J_{\pm\pm}$, the system develops a stripe order, and the spin correlation has a sharp peak at the wave vector M. For smaller spin-orbit coupling, a large number of classical degeneracy will frustrate the system and gives rise to a continuum in the spin correlation. The nearest-neighbor spin interactions are sufficient for reproducing the continuum and peak at M, as evidenced in a recent experimental work [15].

[1] Y. Li, H. Liao, Z. Zhang, S. Li, F. Jin, L. Ling, L. Zhang, Y. Zou, L. Pi, Z. Yang, J. Wang, Z. Wu, and Q. Zhang, Gapless quantum spin liquid ground state in the two-dimensional spin-1/2 triangular antiferromagnet $YbMgGaO_4$, Sci. Rep. **5**, 16419 (2015).

[2] Y. Li, G. Chen, W. Tong, L. Pi, J. Liu, Z. Yang, X. Wang, and Q. Zhang, Rare-Earth Triangular Lattice Spin Liquid: A Single-Crystal Study of $YbMgGaO_4$, Phys. Rev. Lett. **115**, 167203 (2015).

[3] Y.-D. Li, X. Wang, and G. Chen, Anisotropic spin model of strong spin-orbit-coupled triangular antiferromagnets, Phys. Rev. B **94**, 035107 (2016).

[4] Y. Shen, Y.-D. Li, H. Wo, Y. Li, S. Shen, B. Pan, Q. Wang, H. C. Walker, P. Steffens, M. Boehm, Y. Hao, D. L. Quintero-Castro, L. W. Harriger, M. D. Frontzek, L. Hao, S. Meng, Q. Zhang, G. Chen, and J. Zhao, Evidence for a spinon Fermi surface in a triangular-lattice quantum-spin-liquid candidate, Nature **540**, 559 (2016).

[5] J. A. M. Paddison, M. Daum, Z. Dun, G. Ehlers, Y. Liu, M. B. Stone, H. Zhou, and M. Mourigal, Continuous excitations of the triangular-lattice quantum spin liquid $YbMgGaO_4$, Nat. Phys. **13**, 117 (2017).

[6] Y. Li, D. Adroja, P. K. Biswas, P. J. Baker, Q. Zhang, J. Liu, A. A. Tsirlin, P. Gegenwart, and Q. Zhang, Muon Spin Relaxation Evidence for the U(1) Quantum Spin-Liquid Ground State in the Triangular Antiferromagnet $YbMgGaO_4$, Phys. Rev. Lett. **117**, 097201 (2016).

[7] Y. Xu, J. Zhang, Y. S. Li, Y. J. Yu, X. C. Hong, Q. M. Zhang, and S. Y. Li, Absence of Magnetic Thermal Conductivity in the Quantum Spin-Liquid Candidate $YbMgGaO_4$, Phys. Rev. Lett. **117**, 267202 (2016).

[8] Y.-D. Li and G. Chen, Detecting spin fractionalization in a spinon Fermi surface spin liquid, Phys. Rev. B **96**, 075105 (2017).

[9] Y.-D. Li, Y.-M. Lu, and G. Chen, Spinon Fermi surface U(1) spin liquid in the spin-orbit-coupled triangular-lattice Mott insulator $YbMgGaO_4$, Phys. Rev. B **96**, 054445 (2017).

[10] Y.-D. Li, X. Wang, and G. Chen, Hidden multipolar orders of dipole-octupole doublets on a triangular lattice, Phys. Rev. B **94**, 201114 (2016).

[11] Z. Zhu, P. A. Maksimov, S. R. White, and A. L. Chernyshev, Disorder-Induced Mimicry of a Spin Liquid in $YbMgGaO_4$, Phys. Rev. Lett. **119**, 157201 (2017).

[12] Z.-X. Luo, E. Lake, J.-W. Mei, and O. A. Starykh, Spinon Magnetic Resonance of Quantum Spin Liquids, Phys. Rev. Lett. **120**, 037204 (2018).

[13] Y. Li, D. Adroja, R. I. Bewley, D. Voneshen, A. A. Tsirlin, P. Gegenwart, and Q. Zhang, Crystalline Electric-Field Randomness in the Triangular Lattice Spin-Liquid $YbMgGaO_4$, Phys. Rev. Lett. **118**, 107202 (2017).

[14] Y. Li, D. Adroja, D. Voneshen, R. I. Bewley, Q. Zhang, A. A. Tsirlin, and P. Gegenwart, Nearest-neighbor resonating valence bonds in $YbMgGaO_4$, Nat. Commun. **8**, 15814 (2017).

[15] S. Tóth, K. Rolfs, A. R. Wildes, and C. Rüegg, Strong exchange anisotropy in $YbMgGaO_4$ from polarized neutron diffraction, arXiv:1705.05699.

[16] Y. Shen, Y.-D. Li, H. C. Walker, P. Steffens, M. Boehm, X. Zhang, S. Shen, H. Wo, G. Chen, and J. Zhao, Fractionalized excitations in the partially magnetized spin liquid candidate $YbMgGaO_4$, arXiv:1708.06655.

[17] K. A. Ross, L. Savary, B. D. Gaulin, and L. Balents, Quantum Excitations in Quantum Spin Ice, Phys. Rev. X **1**, 021002 (2011).

[18] Y. Shimizu, K. Miyagawa, K. Kanoda, M. Maesato, and G. Saito, Spin Liquid State in an Organic Mott Insulator with a Triangular Lattice, Phys. Rev. Lett. **91**, 107001 (2003).

[19] T. Itou, A. Oyamada, S. Maegawa, M. Tamura, and R. Kato, Spin-liquid state in an organic spin-1/2 system on a triangular lattice, $EtMe_3Sb[Pd(dmit)_2]_2$, J. Phys.: Condens. Matter **19**, 145247 (2007).

[20] Y. Kurosaki, Y. Shimizu, K. Miyagawa, K. Kanoda, and G. Saito, Mott Transition from a Spin Liquid to a Fermi Liquid in the Spin-Frustrated Organic Conductor κ-$(ET)_2Cu_2(CN)_3$, Phys. Rev. Lett. **95**, 177001 (2005).

[21] T. Itou, A. Oyamada, S. Maegawa, M. Tamura, and R. Kato, Quantum spin liquid in the spin-12 triangular antiferromagnet $EtMe_3Sb[Pd(dmit)_2]_2$, Phys. Rev. B **77**, 104413 (2008).

[22] O. I. Motrunich, Variational study of triangular lattice spin-1/2 model with ring exchanges and spin liquid state in κ-$(ET)_2Cu_2(CN)_3$, Phys. Rev. B **72**, 045105 (2005).

[23] S.-S. Lee and P. A. Lee, U(1) Gauge Theory of the Hubbard Model: Spin Liquid States and Possible Application to κ-$(BEDT\text{-}TTF)_2Cu_2(CN)_3$, Phys. Rev. Lett. **95**, 036403 (2005).

[24] W. Witczak-Krempa, G. Chen, Y. B. Kim, and L. Balents, Correlated quantum phenomena in the strong spin-orbit regime, Annu. Rev. Condens. Matter Phys. **5**, 57 (2014).

[25] G. Chen and L. Balents, Spin-orbit effects in $Na_4Ir_3O_8$: A hyper-kagome lattice antiferromagnet, Phys. Rev. B **78**, 094403 (2008).

[26] G. Chen, R. Pereira, and L. Balents, Exotic phases induced by strong spin-orbit coupling in ordered double perovskites, Phys. Rev. B **82**, 174440 (2010).

[27] H. Watanabe, H. C. Po, A. Vishwanath, and M. Zaletel, Filling constraints for spin-orbit coupled insulators in symmorphic and nonsymmorphic crystals, Proc. Natl. Acad. Sci. U. S. A. **112**, 14551 (2015).

[28] A. Olariu, P. Mendels, F. Bert, F. Duc, J. C. Trombe, M. A. de Vries, and A. Harrison, ^{17}O NMR Study of the Intrinsic Magnetic Susceptibility and Spin Dynamics of the Quantum Kagome Antiferromagnet $ZnCu_3(OH)_6Cl_2$, Phys. Rev. Lett. **100**, 087202 (2008).

[29] T.-H. Han, J. S. Helton, S. Chu, D. G. Nocera, J. A. Rodriguez-Rivera, C. Broholm, and Y. S. Lee, Fractionalized excitations in the spin-liquid state of a kagome-lattice antiferromagnet, Nature (London) **492**, 406 (2012).

[30] M. Fu, T. Imai, T.-H. Han, and Y. S. Lee, Evidence for a gapped spin-liquid ground state in a kagome Heisenberg antiferromagnet, Science **350**, 655 (2015).

[31] T.-H. Han, M. R. Norman, J.-J. Wen, J. A. Rodriguez-Rivera, J. S. Helton, C. Broholm, and Y. S. Lee, Correlated impurities and intrinsic spin-liquid physics in the kagome material herbertsmithite, Phys. Rev. B **94**, 060409 (2016).

[32] D. Yamamoto, G. Marmorini, and I. Danshita, Quantum Phase Diagram of the Triangular-Lattice XXZ Model in a Magnetic Field, Phys. Rev. Lett. **112**, 127203 (2014).

[33] D. Sellmann, X.-F. Zhang, and S. Eggert, Phase diagram of the antiferromagnetic XXZ model on the triangular lattice, Phys. Rev. B **91**, 081104 (2015).

[34] C. Liu, R. Yu, and X. Wang, Semiclassical ground-state phase diagram and multi-q phase of a spin-orbit-coupled model on triangular lattice, Phys. Rev. B **94**, 174424 (2016).

[35] D. Bergman, J. Alicea, E. Gull, S. Trebst, and L. Balents, Order-by-disorder and spiral spin-liquid in frustrated diamond-lattice antiferromagnets, Nat. Phys. **3**, 487 (2007).

[36] X. Zhang, F. Mahmood, M. Daum, Z. Dun, J. A. M. Paddison, N. J. Laurita, T. Hong, H. Zhou, N. P. Armitage, and M. Mourigal, Hierarchy of exchange interactions in the triangular-lattice spin-liquid $YbMgGaO_4$, arXiv:1708.07503.